Materials Advances

ROYAL SOCIETY OF CHEMISTRY

PAPER

View Article Online
View Journal | View Issue

Cite this: *Mater. Adv.*, 2022, 3, 4622

Oral drug delivery using a polymeric nanocarrier: chitosan nanoparticles in the delivery of rifampicin†

Ria Ghosh,[ab] Susmita Mondal,[a] Dipanjan Mukherjee,[a] Aniruddha Adhikari,[a] Saleh A. Ahmed,*[cd] Reem I. Alsantali,[e] Abdelrahman S. Khder,[cf] Hatem M. Altass,[c] Ziad Moussa,[g] Ranjan Das,[h] Maitree Bhattacharyya*[b] and Samir Kumar Pal*[a]

Received 14th March 2022,
Accepted 19th April 2022

DOI: 10.1039/d2ma00295g

rsc.li/materials-advances

Oral delivery of drugs is the most common method of drug administration. However, the poor bioavailability of drugs in the systemic circulation makes achieving therapeutic levels *via* the gastrointestinal (GI) tract challenging. Polymeric nanoparticle drug carriers can shield drugs from degradation and deliver them in the upper intestinal region of the GI tract. In this regard, we have developed a nanocarrier from a naturally occurring polymer, chitosan, to investigate its efficacy in a pH-responsive environment to be used as a potential drug delivery vehicle. We have monitored the encapsulation of an anti-tuberculosis drug, rifampicin (RF), to investigate its pH-responsive delivery activity. Although RF is poorly soluble in aqueous media, it is a clinically effective drug due to its ability to inhibit bacterial RNA polymerase. The inescapable necessity and poor solubility automatically necessitate an alternative drug delivery/carrier system. The chitosan nanoparticle system ensures a burst delivery efficiency of 75% of rifampicin at a simulated intestinal pH over a period of 24 hours. Our studies have successfully established the chitosan nanocarrier as a promising oral drug delivery vehicle.

Introduction

In the last decade, the design and development of new drug delivery systems has been relentless, with more emphasis devoted to the development of new methods for controlled drug release.[1] In this regard, polymeric micelles have attracted huge interest in contemporary drug research due to their controlled release and improved stability of drugs in the field of nanomedicine.[1–3] Polymeric drug delivery systems are materials with viscoelastic properties with polymeric networks within them. These hydrophilic polymeric networks improve the solubility of hydrophobic drugs or drugs poorly soluble in water.[4] These drug delivery systems show a reduced uptake by the reticuloendothelial system, thereby protecting the incorporated drug from fast degradation, blood clearance and elimination from the body.[5] The formation and mainly the disintegration of these polymeric systems can be controlled by stimuli-responsive processes, for example pH, ultrasound, temperature, *etc.* In addition to this, the degradation products of these biocompatible polymeric systems can easily be eliminated from the body, after the drug delivery system has fulfilled its task.[6]

Natural biopolymers have been extensively used to prepare responsive drug carrier systems for biomedical applications owing to their biocompatibility, low toxicity and high content of functional groups, which help to make them target-specific by tuning their surface properties. Although significant benefits have been achieved in the relative areas, to the best of our knowledge few studies refer to the formation of bio nanoparticles from natural polymers for the purpose of responsive carrier systems with controlled drug release mechanisms. To date, the active areas of research on drug delivery systems lie in

[a] *Department of Chemical, Biological and Macromolecular Sciences, S. N. Bose National Centre for Basic Sciences, Block JD, Sector III, Salt Lake, Kolkata-700 106, India. E-mail: kpal@bose.res.in*
[b] *Department of Biochemistry, University of Calcutta, 35, Ballygunge Circular Rd, Kolkata, 700019, India. E-mail: sbamitree@gmail.com*
[c] *Department of Chemistry, Faculty of Applied Science, Umm Al-Qura University, 21955 Makkah, Saudi Arabia. E-mail: saahmed@uqu.edu.sa*
[d] *Chemistry Department, Faculty of Science, Assiut University, 71516 Assiut, Egypt*
[e] *Department of Pharmaceutical Chemistry, College of Pharmacy, Taif University, P.O. Box 11099, Taif, 21944, Saudi Arabia*
[f] *Faculty of Science, Chemistry Department, Mansoura University, Mansoura, 35516, Egypt*
[g] *Department of Chemistry, College of Science, United Arab Emirates University, P. O. Box 15551, Al Ain, Abu Dhabi, United Arab Emirates*
[h] *Department of Chemistry, West Bengal State University, Barasat, Kolkata, 700126, India*

† Electronic supplementary information (ESI) available. See DOI: https://doi.org/10.1039/d2ma00295g

the ability to encapsulate and release drugs responding to the acidic environment of tumor tissues (pH 5.5 to 6.0), thereby decreasing undesired drug release during transportation and providing improved effective drug release in the tumor site. However, studies on the release profile of drug molecules responsive in an alkaline environment, overcoming the acidic barrier for oral delivery of drug molecules, are sparse. For this purpose, the mechanism of uptake and release kinetics at different pH values of polymeric micelles can help in the development of biocompatible polymers with tailored properties for oral drug delivery and formulation of nanocarriers.

Herein, we have developed a nanocarrier from a naturally occurring polymer, chitosan, to investigate its efficacy in a pH-responsive environment to be used as a potential drug delivery vehicle. We have monitored the mechanism by encapsulating an anti-tuberculosis drug, rifampicin (RF), to investigate its pH-responsive delivery activity. Although RF is poorly soluble in aqueous media, it is a clinically effective drug due to its ability to inhibit bacterial RNA polymerase.[7] The inescapable necessity and poor solubility automatically necessitate an alternative drug delivery/carrier system.[7] In this regard, the interaction of RF with the prepared chitosan nanocarrier is essential. The synthesized chitosan nanocarrier is characterized using electron microscopic techniques like TEM. We have monitored the binding of RF at pH 7 by using time-resolved fluorescence spectroscopy by labelling the nanocarrier with a fluorescent probe, Acyman. Förster resonance energy transfer (FRET) between the FRET pair Acyman (incorporated to chitosan nanocarriers) and RF (encapsulated within the chitosan nanocarrier system) has successfully manifested the efficiency of binding of RF with chitosan. Based on the microstructural changes of the chitosan nanocarrier, the *in vitro* drug release profile of the drug molecule (RF) has been studied through a dialysis method at various pH values. To mimic the normal physiological conditions, the delivery efficacy of the synthesized chitosan nanocarrier has also been evaluated in simulated gastric and intestinal media. Hence, we have successfully established the RF-encapsulated chitosan nanocarrier as a promising and model oral drug delivery vehicle.

Materials and methods

Chemicals

Analytical grade chemicals were used without further purification. Chitosan (M_w ~ 150 000, degree of deacetylation ~75%), tripolyphosphate (TPP) and rifampicin (RF) were purchased from Sigma Aldrich. The experimental procedure for the synthesis of the Acyman dye has been described earlier.[8] All the chemicals were used as obtained from the respective manufacturers. Ethanol (Merck) and Milipore water were employed as solvents. To maintain the pH of the solutions, buffer solutions were used, namely glycine–HCl buffer (pH 2), acetate buffer (pH 4) phosphate buffer solutions (pH 7, pH 8) and glycine–NaOH buffer solutions (pH 10).

Synthesis of chitosan nanoparticles

Chitosan nanoparticles were prepared according to the ionotropic gelation method using TPP anions.[9] Briefly, chitosan was dissolved in 1% (w/v) acetic acid followed by stirring at 200 rpm. TPP was dissolved in 1% (w/v) ultrapure water. Blank chitosan nanoparticles were prepared by crosslinking of chitosan with TPP with final concentrations of 0.5 and 2 mg ml^{-1}, respectively, under stirring conditions. The resulting formulations were subjected to centrifugation at 5000 rpm and the pellets were resuspended in ultrapure water followed by sonication (with a 30 mm probe, sonicator) at 80% pulse ratio. According to the previously reported literature, the nanoparticles were formed due to the interaction between the negative groups of TPP and the positively charged groups of chitosan.[9–12]

Preparation of the chitosan–RF complex

RF was added to the chitosan solution to a final concentration of 2% (w/v). TPP was then added to the chitosan–RF solution under stirring conditions. To remove the free drug molecules, the chitosan nanoparticle–RF complex was centrifuged at 5000 rpm for 2 minutes and the resultant pellet was resuspended in ultrapure water. RF loading was calculated spectrophotometrically at 450 nm. The entrapment efficiency (EE) was calculated using the following equation:

$$\text{EE}\ (\%) = \frac{\text{Total drug} - \text{free drug}}{\text{Total drug}} \times 100 \qquad (1)$$

To calculate the drug loading capacity of the synthesized chitosan nanocarriers, firstly a dried nanoparticle product was obtained by freeze drying the nanoparticles, followed by lyophilisation. The percentage of loading capacity (LC) of the nanoparticles was calculated using the formula:

$$\text{LC}\ (\%) = \frac{\text{Total drug} - \text{free drug}}{\text{Nanoparticle weight}} \times 100 \qquad (2)$$

The concentration of the drug was measured from the prepared calibration curve. All the experiments were performed in triplicate (n = 3).

Release studies

Drug release experiments were performed using the modified dialysis method.[13] The chitosan nanoparticle–RF complex was introduced to a cellulose dialysis membrane. The dialysis membrane then was immersed in 30 ml of acetate buffer (pH 4) or phosphate buffer (pH 7 or pH 8) in a beaker that served as the receiver fluid maintaining sink conditions. The entire setup was kept under stirring conditions, at a mixing speed of 330 rpm to enable mixing inside the beaker, and a hot plate was used to maintain the temperature inside the beaker at 37 °C. The quantity of RF was adjusted to obtain a maximum RF concentration of 1 μg ml^{-1}. At varying time points, 2 ml of the buffer was collected and the concentration of RF was calculated spectrophotometrically as described earlier. The amount of drug released at each time interval was determined with

reference to the standard curve. A similar volume (2 ml) of the buffer was added to the sink after each successive time point to maintain the overall volume of the sink at 30 ml at each time point.

To monitor the release kinetics in simulated environments, simulated gastric fluid (SGF) and simulated intestinal fluid (SIF) were used instead of the buffer solutions. SGF was prepared using 70 mM HCl, 34.2 mM NaCl and Milli-Q water, and the pH was adjusted to 2 ± 0.1. SIF was prepared using 75 mM potassium monobasic phosphate and 13 mM SDS, and the pH was adjusted to 8.0 ± 0.1 with 1 N NaOH. The release kinetics of RF from the nanoparticles was monitored by collecting 2 ml of the fluid at specific time points and was replenished with fresh SGF and SIF to maintain the overall volume of the sink. The concentration of RF in the collected buffer was obtained from its absorbance peak at 450 nm as described earlier.

The release efficiency (RE) was calculated according to the formula:

$$\mathrm{RE} = (A_t/A_{\mathrm{encapsulated}}) \times 100 \quad (3)$$

where A_t is the absorbance of rifampicin at 450 nm at time t.

All the experiments at each pH value were conducted three times (n = 3) and the results were expressed in terms of their mean ± standard deviation described in the later section.

Fitting of the release kinetic studies

In this study, the experimental data obtained from the dialysis studies are fitted according to the Korsmeyer Peppas equation:[14]

$$\frac{M_t}{M_\infty} = Kt^n \quad (4)$$

where M_t/M_∞ represents the fractional amount of the drug permeated through the membrane at time t; K is the transport constant and n is the transport exponent. It is to be noted that as the main aim was to investigate the mathematical model of drug release from the nanocarriers, the Korsmeyer–Peppas model was chosen as it provides descriptive information about both the release kinetics and mechanism of drug release.[15] The fitted data represent the diffusion through the retention barriers along with the release kinetics from the nanocarriers. The parameter K is directly proportional to the drug release kinetics, which indicates the faster or slower transport kinetics of the drug from the nanocarriers.

Characterization

Dynamic light scattering (DLS). DLS was used to measure the average hydrodynamic diameter and polydispersity index (PDI) of the nanoparticles using a zetasizer Nano S DLS instrument (Malvern, UK), equipped with a 4 mW He:Ne laser (l = 632.8 nm) and a thermostatted sample chamber.[16] Millipore water was used as the reference for the dispersing medium. All the measurements were performed in batches of triplicates.

Transmission electron microscopy (TEM). TEM was used to examine the morphology of the nanoparticles prepared in this study. Nanoparticle samples were deposited on copper grids and coated with lead citrate. The solutions were dried at ambient temperature before observation. After evaporation, the samples were visualized under transmission electron microscopy using a Tecnai S-Twin, operating at 200 kV.[17]

Differential scanning calorimetry (DSC). DSC analysis was performed using a Netzsch DSC 204 F1 instrument to evaluate the thermal properties of the synthesised nanoparticles. The heating curves were recorded by heating the samples from −40 °C to 200 °C at a rate of 10 °C min^{-1}. Subsequently, the cooling curves were recorded when the samples were cooled from 200 °C to −40 °C at a rate of 10 °C min^{-1}.

X-Ray diffraction (XRD) studies. The X-ray diffraction (XRD) patterns of the samples were recorded using a PANalytical XPERTPRO diffractometer equipped with Cu Kα radiation (at 40 mA and 40 kV). The samples were scanned at a rate of 0.02° S^{-1} at a 2θ range from 20° to 80°.

FTIR studies

For Fourier transform infrared spectroscopy (FTIR) experiments, the sample was dropcast on an ATR stage of a FTIR-spectrometer (Vertex 70V, Bruker, Germany).

Spectroscopic studies

A Shimadzu spectrophotometer (UV2600) was used for measuring the absorbance spectra of the RF and chitosan RF conjugates. The fluorescence emission and excitation spectra were measured using a spectrofluorometer, Model FP-8200 (Jasco, Tokyo, Japan). Picosecond-resolved fluorescence transients were measured by using a commercially available spectrophotometer (Life Spec-ps) from Edinburgh Instruments, UK as reported in our earlier publications.[18]

Förster resonance energy transfer study

The FRET distance between donor–acceptor (r) was calculated from the equation:

$$r^6 = R_0{}^6(1 - E)/E \quad (5)$$

where E is the efficiency of the energy transfer between the donor and acceptor and calculated using the equation:

$$E = 1 - \tau_{\mathrm{DA}}/\tau_{\mathrm{D}} \quad (6)$$

where τ_{DA} and τ_{D} are the fluorescence lifetimes of the donor in the presence and absence of the acceptor. The Förster distance (R_0) was calculated using the overlap integral of the emission spectrum of the donor and absorption spectrum of the acceptor following the equation in Å, where κ^2 is the factor describing the relative orientation in space of the transition dipoles of the donor and the acceptor. The magnitude of κ^2 is assumed to be 0.66 for random orientation of the donor and the acceptor. The refractive index (η) of the biological medium is assumed to be 1.4. $J(\lambda)$ is the overlap integral of emission of the donor and absorption of the acceptor and calculated by:

$$J(\lambda) = \frac{\int_0^\infty F_{\mathrm{D}}(\lambda)\varepsilon_{\mathrm{A}}(\lambda)\lambda^4 \mathrm{d}\lambda}{\int_0^\infty F_{\mathrm{D}}(\lambda)\mathrm{d}\lambda} \quad (7)$$

where $F_D(\lambda)\,d\lambda$ is the fluorescence emission of the donor in the wavelength region λ to $\lambda + d\lambda$. $\varepsilon(\lambda)$ is the extinction coefficient (in $M^{-1}\,cm^{-1}$) of the acceptor.[16,18]

XRD

Statistical analysis. All quantitative data are expressed as mean ± standard deviation (SD) unless otherwise stated. Standard deviation between the successive outcomes of the same experiment was measured using the formula:

$$SD = \sqrt{\frac{\sum_{i=0}^{N}(x_i - \mu)}{N}} \quad (8)$$

where N refers to the number of experimental outcomes, μ is the mean of the individual outcomes and x_i is each outcome of the experiment.

One-way analysis of variance followed by Tukey's multiple comparison tests was executed for comparison of different parameters between the groups using a computer program. GraphPad Prism (version 5.00 for Windows), GraphPad Software, California, USA. $p < 0.05$ was considered significant.

Results and discussion

Characterization of the chitosan- and rifampicin-loaded nanoparticles

Chitosan (CS) nanoparticles were formed by the ionic gelation method. CS molecules are in the form of a cationic polyelectrolyte in solution, which tends to form specialised structures through electrostatic interactions with the phosphate groups of TPP and lead to the formation of polymeric nanoparticles, *via* the polymerization of the CS in the presence of TPP as a crosslinker. Although the electrostatic interactions play a major role in the polymerization reaction, other interactions such as the hydrophobic association of the polymer chains proceeding with TPP has also been known to contribute towards the stability of the nanoparticles. TEM micrographs confirm the homogeneous distribution of spherical nanoparticles (Fig. 1a) with an average size distribution of 9.84 ± 0.23 nm (Fig. 1b). The hydrodynamic diameter of the particles was found to be ~10 nm, which is consistent with the TEM observation. This relatively small size of the nanoparticles may be accounted for by the compact structure of the nanoparticles owing to a higher degree of neutralization of the charged amino groups, thereby leading to weakened charge repulsion between the CS and the TPP ions.

XRD patterns of chitosan and rifampicin-loaded chitosan nanoparticles are shown in Fig. S1 (ESI†). Chitosan has two strong 2θ peaks at 10.4° and 21.8°, corresponding to the crystallinity of chitosan.[19] However, no such peaks were observed in the chitosan nanoparticles or rifampicin-loaded chitosan nanoparticles. No significant differences were obtained between the diffractograms of the chitosan nanoparticles and rifampicin-loaded chitosan nanoparticles, indicating that chitosan is an amorphous polymer, corroborating with the TEM studies (Fig. 1a inset).

The DSC thermogram of the nanocarrier is presented in the ESI,† Fig. S2. The DSC thermogram of the chitosan nanocarrier displays two exothermic peaks at 5 °C and 117 °C. The first peak may be accredited to the loss of bound and absorbed water and the second peak may correspond to its degradation. The thermogram of rifampicin is characterized by a small exothermic peak at 84 °C, which could be due to its melting point.

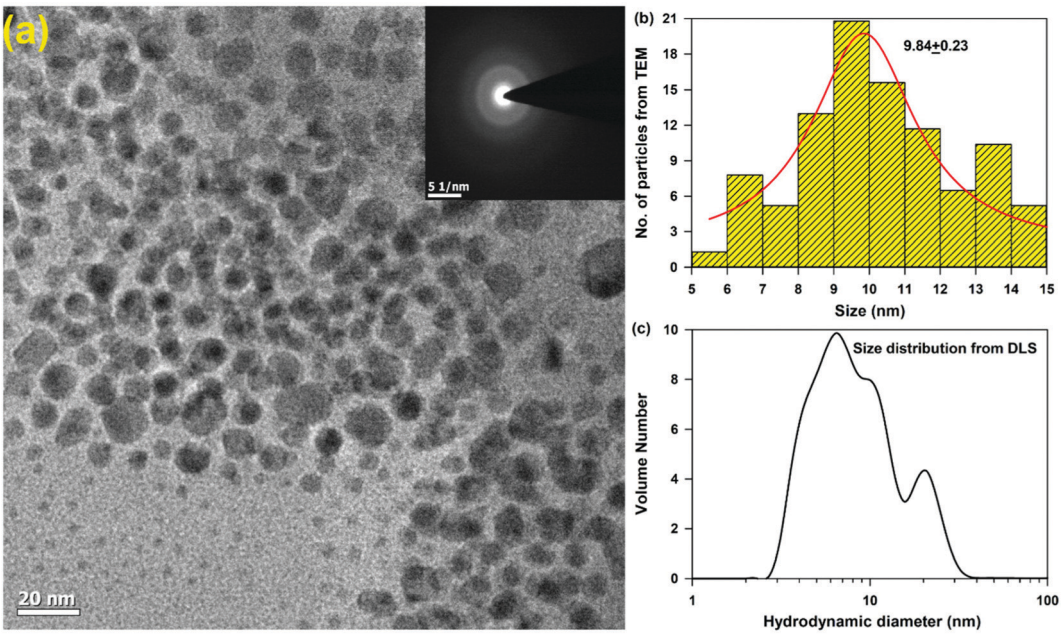

Fig. 1 Size of the synthesised chitosan nanocarriers. (a) TEM micrograph of the synthesised chitosan nanoparticles. The SAED image of the nanoparticles (inset), (b) size distribution and (c) hydrodynamic diameter.

This peak is also present in the thermogram of the rifampicin-loaded nanoparticles, which verifies the encapsulation of rifampicin in the chitosan nanocarriers and their existence in an amporphous state. In addition, the peak at 109 °C in the thermogram of the rifampicin-loaded nanoparticles represents the degradation peak of chitosan. Thus, the nanocarrier is stable at the physiological temperature and does not cause any precipitation in the physiological milieu.

Loading and release studies

The loading of a model drug (rifampicin) in the chitosan nanoparticles was confirmed using the FRET technique. FRET is an effective technique to find out the distance between two ligands having overlap in their emission and absorption spectra. We studied the resonance energy transfer between the ligands Acyman and rifampicin in the chitosan nanoparticles. Energy transfer within the nanoparticle system between the donor (Acyman) and the acceptor (rifampicin) will only take place under the simultaneous binding of these molecules to the nanoparticles without any restriction of the relative orientation of their dipole moments, thereby confirming the localization of the drug molecule (rifampicin) to the nanoparticles. Fig. 2a illustrates the spectral overlap between the emission spectrum of Acyman bound to chitosan nanoparticles and the absorption spectrum of rifampicin. The huge spectral overlap suggests that an efficient FRET between the donor (Acyman) and the acceptor (rifampicin) can take place. Fig. 2b (inset) reveals a significant quenching of the steady-state fluorescence intensity of Acyman complexed with chitosan nanoparticles (emission peak 460 nm) in the Acyman-rifampicin complex on exciting at 409 nm. These observations are confirmed by the fluorescence lifetime measurements, where a substantial shortening of the Acyman donor lifetime is measured in the presence of rifampicin complexed with the chitosan nanoparticles (Fig. 2b). Analysis of the above-mentioned temporal fluorescence decay shows that the distance between the donor and the acceptor has been estimated to be 5.02 nm with an energy transfer efficiency of 50.7%, by using an R_0 value of 5.67 nm. This observation is consistent with the binding of the donor and acceptor across the chords in the spherical chitosan nanoparticle (10 nm diameter). This confirms the loading of the rifampicin drug molecule on the chitosan nanoparticles. The loading efficiency of nanoparticles was found to be 9.5% with an encapsulation efficiency of 43%, as calculated from eqn (1) and (2), respectively. It has to be noted that FTIR studies confirmed that no possible interaction was present between the drug (rifampicin) and the excipient (Fig. S3, ESI†) that could interfere with the delivery efficacy of the carrier.

The release kinetics profile from the chitosan nanoparticles was evaluated in pure water and in different pH conditions (Fig. 3a). A burst release profile of rifampicin from the chitosan

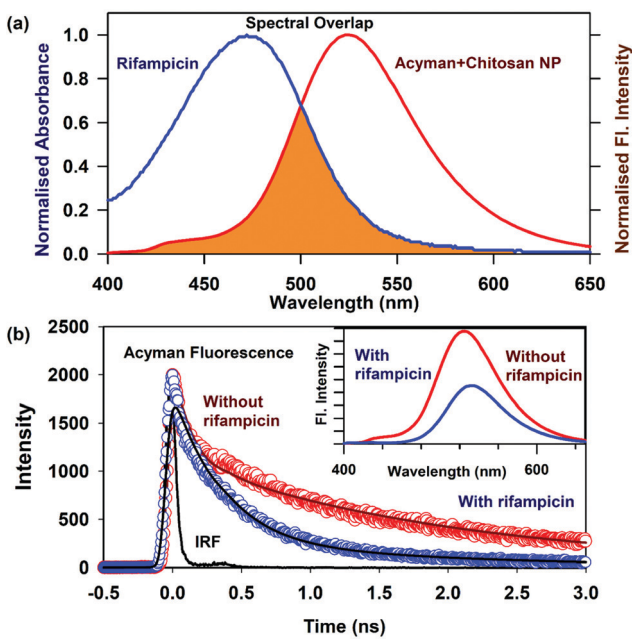

Fig. 2 Loading of rifampicin in the chitosan nanocarriers by FRET studies. (a) Spectral overlap of Acyman in chitosan nanoparticles with rifampicin, and (b) pico-second-resolved fluorescence transients. Steady state fluorescence spectra of Acyman with chitosan nanoparticles with and without rifampicin drug (inset).

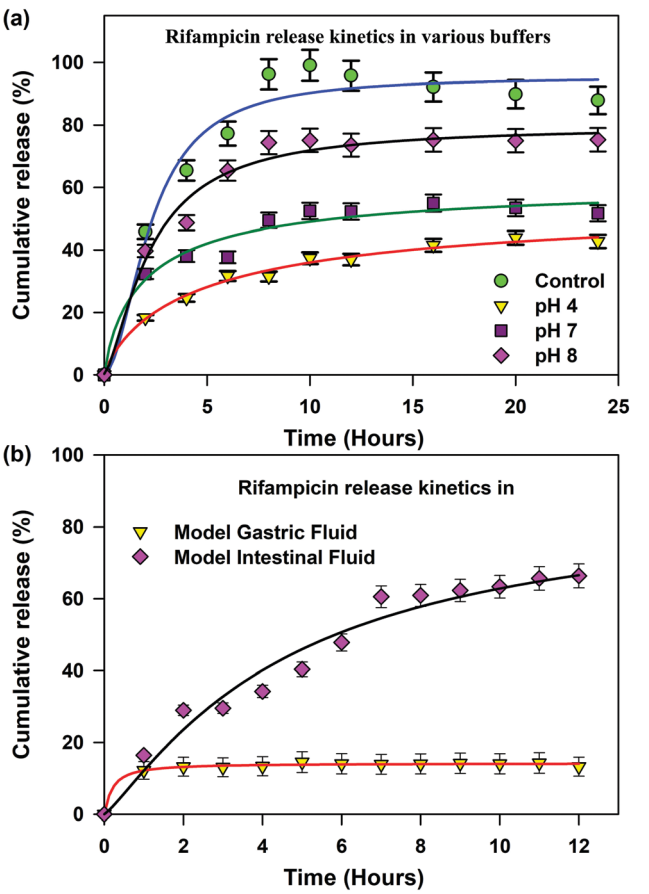

Fig. 3 Release studies of rifampicin from the chitosan nanocarriers. (a) Release profiles of rifampicin in different pH media. (b) Release profiles of rifampicin in simulated pH media. The error bars represent the standard deviation of each experimental data point (n = 3).

nanoparticles was observed both in the acidic (pH 4) and alkaline pH (pH 8). Release of rifampicin in pure water (control) reached equilibrium in 5 hours, while in the acidic medium (pH 4), the release of rifampicin was exceptionally slow with a maximum release efficiency of 40% after 24 hours of dialysis. However, the release profile of rifampicin was pronounced at the alkaline pH (pH 8) with a release efficiency of 70% after 24 hours. Hence, the nanoparticle can be an effective oral delivery agent that could bypass the acidic medium of the stomach with significant delivery in the small intestine (alkaline pH). The experimental diffusion data were fitted according to the Korsmeyer Peppas equation. For all the data sets, the correlation coefficient (R^2) was between 0.9 and 0.95 indicating a good correlation with the experimental data. The transport constant K (K = 25), was much higher in the alkaline pH (pH 8) indicating a faster drug release. On the contrary, a lower value of K (K = 10) in the acidic medium represents slow transport kinetics and a poor drug release from the nanocarrier.[20] Thus, the nanocarrier showed promising oral delivery activity by slower kinetic release of the drug molecules in the acidic pH and thereby, preventing the drug from degradation in the acidic medium.

To have a more realistic insight into the release profile of rifampicin from chitosan nanoparticles, we studied the release kinetics in a simulated gastric and alkaline environment (Fig. 3b). Chitosan nanoparticles showed a higher delivery efficiency of 75% in the simulated alkaline environment in comparison to the simulated acidic environment of less than 10%, which was consistent with our previous studies. This alteration in behaviour is dependent on the charging properties and the interplay between the chitosan and the TPP molecules. At a low pH, most of the amino groups of the chitosan are protonated, enabling the chitosan molecules to exhibit an extended conformation due to strong charge repulsion. The TPP molecules are also protonated, leading to lower charging density of the molecules. At pH 4, the TPP molecules are sufficiently deprotonated and the degree of protonation of chitosan is less influenced. Thus, the charge interaction between these two molecules becomes strong enough, thereby not allowing the release of rifampicin molecules within the core of the chitosan nanoparticles. At neutral pH (Fig. 3a), the ions in the medium could screen the charge interaction between both the chitosan and TPP, thereby leading to a release efficiency of 40%. However, at a higher pH (pH 8) the charging degree of TPP is greatly enhanced, which neutralises the charge density in chitosan to a great extent, thereby leading to the collapse of the nanoparticle structure and release of the rifampicin molecule.

Conclusions

We have developed a nanocarrier from a chitosan polyelectrolyte solution with an average diameter of 10 nm to investigate its efficacy in a pH-responsive environment to be used as a potential drug delivery vehicle. We have encapsulated rifampicin within the core of the synthesized nanoparticles and evaluated its pH-dependent delivery efficiency. The nanoparticles showed a maximum delivery efficiency of rifampicin in the alkaline environment (pH 8) in comparison to the acidic (pH 4) or neutral environment (pH 7). Based on the changes of the chitosan nanocarrier, and *in vitro* drug release profile of rifampicin from the chitosan nanoparticles, our studies indicate chitosan nanoparticles as a promising oral drug delivery vehicle.

Conflicts of interest

The authors declare no conflict of interest.

Acknowledgements

SKP thanks the Indian National Academy of Engineering (INAE) for the Abdul Kalam Technology Innovation National Fellowship, INAE/121/AKF. The authors would like to extend their sincere appreciation to Taif University Researchers Supporting Project number (TURSP-2020/312), Taif University, Taif, Saudi Arabia. Dr Ziad Moussa is grateful to the United Arab Emirates University (UAEU) of Al-Ain and to the Research Office for supporting the research developed in his laboratory (Grant no. G00003291). The authors would like to acknowledge the Deanship of Scientific Research at Umm Al-Qura University, for supporting this work by Grant code: 22UQU4320545DSR11.

References

1 A. Kumari, S. K. Yadav and S. C. Yadav, Biodegradable polymeric nanoparticles based drug delivery systems, *Colloids Surf., B*, 2010, **75**(1), 1–18.
2 G. S. Kwon and K. Kataoka, Block copolymer micelles as long-circulating drug vehicles, *Adv. Drug Delivery Rev.*, 2012, **64**, 237–245.
3 G. S. Kwon and T. Okano, Polymeric micelles as new drug carriers, *Adv. Drug Delivery Rev.*, 1996, **21**(2), 107–116.
4 K. Ghosal, *et al.*, Novel interpenetrating polymeric network based microbeads for delivery of poorly water soluble drug, *J. Polym. Res.*, 2020, **27**(4), 1–11.
5 K. Knop, *et al.*, Poly (ethylene glycol) in drug delivery: pros and cons as well as potential alternatives, *Angew. Chem., Int. Ed.*, 2010, **49**(36), 6288–6308.
6 N. Kamaly, *et al.*, Degradable controlled-release polymers and polymeric nanoparticles: mechanisms of controlling drug release, *Chem. Rev.*, 2016, **116**(4), 2602–2663.
7 T. Mondol, *et al.*, Interaction of an antituberculosis drug with a nanoscopic macromolecular assembly: temperature-dependent Forster resonance energy transfer studies on rifampicin in an anionic sodium dodecyl sulfate micelle. The, *J. Phys. Chem. B*, 2011, **115**(12), 2924–2930.
8 S. Singha, *et al.*, A structural remedy toward bright dipolar fluorophores in aqueous media, *Chem. Sci.*, 2015, **6**(7), 4335–4342.
9 E. N. Koukaras, *et al.*, Insight on the formation of chitosan nanoparticles through ionotropic gelation with tripolyphosphate, *Mol. Pharmaceutics*, 2012, **9**(10), 2856–2862.

10 W. Fan, *et al.*, Formation mechanism of monodisperse, low molecular weight chitosan nanoparticles by ionic gelation technique, *Colloids Surf., B*, 2012, **90**, 21–27.
11 S. A. Algharib, *et al.*, Preparation of chitosan nanoparticles by ionotropic gelation technique: Effects of formulation parameters and in vitro characterization, *J. Mol. Struct.*, 2022, **1252**, 132129.
12 F. Khoerunnisa, *et al.*, Physicochemical Properties of TPP-Crosslinked Chitosan Nanoparticles as Potential Antibacterial Agents, *Fibers Polym.*, 2021, **22**(11), 2954–2964.
13 P. Patil, P. Joshi and A. Paradkar, Effect of formulation variables on preparation and evaluation of gelled self-emulsifying drug delivery system (SEDDS) of ketoprofen, *AAPS PharmSciTech*, 2004, **5**(3), 43–50.
14 I. Y. Wu, *et al.*, Interpreting non-linear drug diffusion data: Utilizing Korsmeyer-Peppas model to study drug release from liposomes, *Eur. J. Pharm. Sci.*, 2019, **138**, 105026.
15 S. Gooneh-Farahani, S. M. Naghib and M. R. Naimi-Jamal, A novel and inexpensive method based on modified ionic gelation for pH-responsive controlled drug release of homogeneously distributed chitosan nanoparticles with a high encapsulation efficiency, *Fibers Polym.*, 2020, **21**(9), 1917–1926.
16 P. Singh, *et al.*, Probing relaxation dynamics of a cationic lipid based non-viral carrier: A time-resolved fluorescence study, *RSC Adv.*, 2019, **9**(61), 35549–35558.
17 D. Bagchi, *et al.*, NIR-light-active ZnO-based nanohybrids for bacterial biofilm treatment, *ACS Omega*, 2018, **3**(9), 10877–10885.
18 D. Mukherjee, *et al.*, Decoding the Kinetic Pathways toward a Lipid/DNA Complex of Alkyl Alcohol Cationic Lipids Formed in a Microfluidic Channel, *J. Phys. Chem. B*, 2022, **126**(3), 588–600.
19 L. Qi, *et al.*, Preparation and antibacterial activity of chitosan nanoparticles, *Carbohydr. Res.*, 2004, **339**(16), 2693–2700.
20 A. V. Sorokin, V. A. Kuznetsov and M. S. Lavlinskaya, Synthesis of graft copolymers of carboxymethyl cellulose and N,N-dimethylaminoethyl methacrylate and their study as Paclitaxel carriers, *Polym. Bull.*, 2021, **78**(6), 2975–2992.